

# GFT: Graph Feature Tuning for Efficient Point Cloud Analysis

Manish Dhakal<sup>†</sup>, Venkat R. Dasari<sup>§</sup>, Rajshekhar Sunderraman<sup>†</sup>, Yi Ding<sup>†</sup>

<sup>†</sup>Department of Computer Science, Georgia State University, Atlanta, GA

<sup>§</sup>DEVCOM Army Research Laboratory, Aberdeen Proving Ground, MD

mdhakal3@gsu.edu, venkateswara.r.dasari.civ@army.mil, rsunderraman@gsu.edu, yiding@gsu.edu

## Abstract

Parameter-efficient fine-tuning (PEFT) significantly reduces computational and memory costs by updating only a small subset of the model’s parameters, enabling faster adaptation to new tasks with minimal loss in performance. Previous studies have introduced PEFTs tailored for point cloud data, as general approaches are suboptimal. To further reduce the number of trainable parameters, we propose a point-cloud-specific PEFT, termed Graph Features Tuning (GFT), which learns a dynamic graph from initial tokenized inputs of the transformer using a lightweight graph convolution network and passes these graph features to deeper layers via skip connections and efficient cross-attention modules. Extensive experiments on object classification and segmentation tasks show that GFT operates in the same domain, rivalling existing methods, while reducing the trainable parameters. Code is available at <https://github.com/manishdhakal/GFT>.

## 1. Introduction

Earlier methods of point cloud modeling include PointNet [20], PoinNet++ [21], and DGCNN [30]. These methods utilize the global and local features from point clouds in  $(x, y, z)$  coordinates space, yielding significant performance in classification and segmentation. However, there has been evidence that these point cloud representation learning methods may not be optimal due to random initialization of weights [5, 19, 37]. One approach to fixing these issues is to perform self-supervised pretraining and full fine-tuning (FFT) for some downstream tasks. This has been demonstrated to be effective in various works [16, 17, 35].

FFT of the pretrained models is expensive, as a separate copy of the fine-tuned model is required to be stored for every new additional tasks. It demands more storage expense for horizontal scaling of the tasks and reduces the degree of parameters sharing. To overcome this issue, various parameter-efficient fine-tuning (PEFT) methods—such as Adapters [11], and VPT [14],—have been developed for

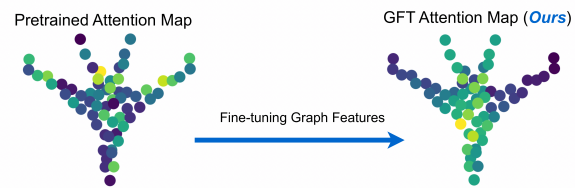


Figure 1. Attention maps (top-view) from the last layer with an airplane point cloud: Brighter points indicate patches contributing more to the global feature. The pretrained transformer (left) is random and uneven, while the GFT (right) shows more uniform regional pooling. Additional visualizations of different objects are included in the supplementary (Section 11).

pretrained transformers [28] networks. These PEFTs have shown significant improvement in fine-tuning language and computer vision tasks. However, Zhou et al. [44] exhibited the sub-optimality of these generic PEFTs to adapt downstream tasks for point cloud analysis, implying a need for PEFTs specific to point cloud [38, 44]. IDPT [38] and DAPT [44] rose as point-cloud-specific PEFTs to fine-tune downstream tasks.

Learning graph features within the tokens of transformers has been an intuitive approach for fine-tuning transformer [28] models. The motivations for incorporating graph features stems from the transformer architecture itself, where self-attention can be interpreted as a fully connected, dynamic graph with a complexity of  $\mathcal{O}(n^2)$  over  $n$  tokens, and the attention maps serve as edge weights. For efficiency, we can make this dynamic graph update sub-quadratic or linear with  $k\mathcal{O}(n)$  complexity ( $k \ll n$ ) via KNN graphs. Additionally, Figure 1 demonstrates the effectiveness of fine-tuning graph features, as it rewrites the attention maps to capture discriminative local geometric structures—effectively learning where to focus. In contrast, the attention maps from the pretrained model appear random and scattered, lacking a clear sense of focus.

IDPT [38] employs a heavy graph features learner only in the model’s final layer. However, this approach has a sig-

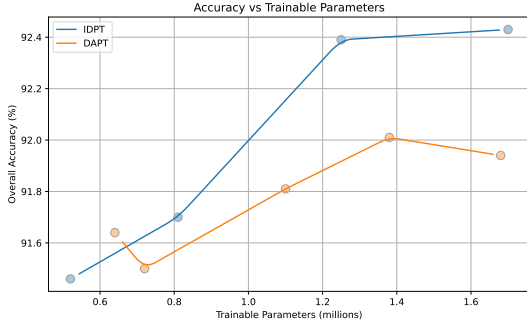


Figure 2. Within the parameter budget of  $(0.6M, 1.7M)$ , baselines (IDPT and DAPT) exhibited maximum drops of 0.97% and 0.51%, respectively, when evaluated with OBG\_BJ dataset. Another ablation at Figure 5 compares our method with the baselines regarding performance-efficiency trade-off.

nificant drawback: the model is relatively heavy and sensitive to parameter budget reduction (as shown in Figure 2). Our goal is to design a lightweight and point-cloud-specific PEFT that can learn graph features for fine-tuning while being parameter-budget-friendly.

With this study, we propose *Graph Features Tuning* (*GFT*) that incorporates additional graph features from the transformer’s input tokens to the deeper layers of the model, as shown in Figure 3. *GFT* introduces three modules that adapt downstream tasks: **(1) Task-specific prompt** [14] module that prepends learnable continuous token to token embedding space for higher degree of freedom for the graph. **(2) EdgeConv** [30] module has multiple layers of graph convolutional network (GCN) that embed locality information. **(3) Cross-attention interaction** module injects the graph features into the encoder. All of these modules are extremely small, updating merely 0.73 million parameters to fine-tune a pretrained transformer for classification.

In summary, we highlight our major contributions as:

- We propose Graph Feature Tuning (*GFT*), a novel fine-tuning method specifically designed for point cloud data, which achieves state-of-the-art parameter efficiency to the best of our knowledge.
- Through extensive experiments and ablation studies, we systematically analyze the performance-efficiency trade-off, demonstrating that *GFT* maintains competitive accuracy while significantly reducing the number of trainable parameters compared to existing benchmarks.

## 2. Related Work

### 2.1. Representation Learning of Point Clouds

Earlier self-supervised models used convolution-like operators [30, 32] to pass messages between points and their neighbours [29, 40, 41] for representation learning. With the rise of Transformers [28], Point Transformers [42] have

been devised to encode a group of points as a single token, and multiple sequential tokens were used as inputs for stacked self-attention networks [5, 19, 22, 37, 39]. Following the principles of masked language modeling, most of the self-supervised point cloud models learn from masked point modeling that randomly masks points from the cloud and enforces the models to predict the missing signal. Point-BERT [37] learns to generate discrete point tokens containing meaningful information about the missing signals by using discrete Variational AutoEncoder (dVAE). Point-MAE [19], PointM2AE [39], and ReCon [22] have shown significant improvement in the pertaining process by reconstructing the missing information. ACT [5] learns the representation with self-supervision by employing cross-modal transfer of weights from a 2D image or language encoder. In our work, we use the pretrained models with architectures based on point transformers trained with different reconstruction methods and a variety of pertaining recipes.

### 2.2. Parameter Efficient Fine-Tuning for Point Clouds

Parameter-efficient fine-tunings (PEFTs) modulate the representation of the pretrained models with addition of fewer learnable parameters for the downstream tasks. Adapters update pretrained models by training smaller blocks that runs in parallel to pretrained blocks [11, 25], effectively fine-tuning vision and language tasks [4, 11, 12, 33]. Prompt tuning, on the other hand, introduces learnable continuous tokens into the transformer’s embedding space while keeping the pretrained model frozen [1, 6, 14, 26, 43]. Although these PEFT methods have demonstrated success in vision and language domains, they fall short in point cloud analysis [38, 44]. To address this, two PEFT approaches have been specifically designed for point clouds: IDPT [38] and DAPT [44]. IDPT learns prompts from the last layer by generating a graph between tokens, while DAPT fine-tunes adapters by generating a dynamic scale for each token. In this work, we propose a PEFT that further optimizes efficiency for point cloud tasks.

### 2.3. Message Passing in Point Cloud

Message passing from neighboring data to generate local features is straightforward for text and 2D images because they inherently possess structural information. In these domains, convolutional operators can efficiently aggregate information from neighboring elements within the feed-forward network [3, 9, 15]. However, point clouds lack such structural information, as they are represented as an unordered set of  $xyz$  coordinates. To enable convolution-like message passing, a graph-based structure is required to define relationships between points, typically using K-nearest neighbors (KNN) [21, 30]. In this work, we utilize EdgeConv [30] to encode locality features from the token

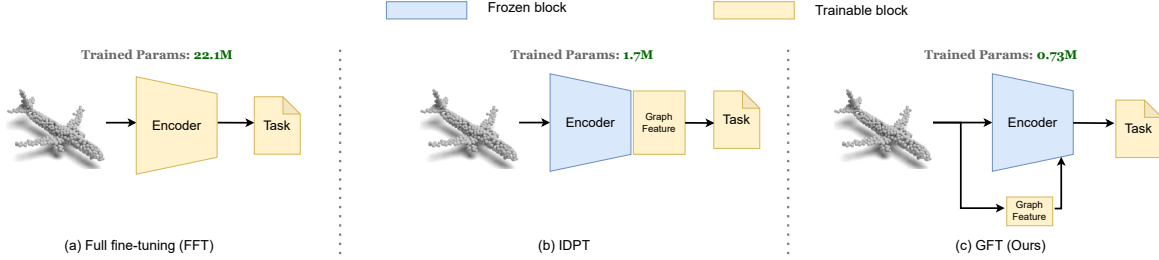


Figure 3. **Full fine-tuning (FFT) vs. IDPT [38] vs. GFT. (classification task)** (a) The whole model is fine-tuned in an end-to-end manner, including the encoder and the task head. (b) IDPT freezes the encoders and trains a *heavy* graph feature extractor at the last layer. (c) With *light* blocks, GFT extracts graph features from the earliest tokens of transformers and selectively injects features into the encoder.

space of the transformer, allowing for effective locality feature extraction.

### 3. Methodology

#### 3.1. Preliminary of Point Transformer

Point Transformer [42] encodes 3D points  $x \in \mathbb{R}^{N \times 3}$  from  $(x, y, z)$  space to  $D$ -dimensional latent space. It contains two major components: a point tokenizer that divides the entire  $N$  points into  $L$  tokens and  $F$  (usually  $F = 12$ ) transformer encoder layers with self-attention mechanisms.

First, the point tokenizer selects  $L$  token centroids with the farthest point sampling (FPS) method from the entire set of points. Then, each center samples its  $K$ -nearest neighbours to embed the locality information, forming the  $L$  tokens as  $x' \in \mathbb{R}^{L \times k \times 3}$ . Each of the token is projected to  $D$  dimension space to form a 1-dimensional grouped point representation as a matrix of shape  $\mathbb{R}^{L \times D}$ . A classification token,  $T_{cls} \in \mathbb{R}^{1 \times D}$ , is prepended to the tokens which give the initial embedding matrix:

$$E_0 = [T_{cls}; [T_1, T_2, T_3, \dots, T_L]], \quad (1)$$

where  $E_0 \in \mathbb{R}^{(1+L) \times D}$ . This embedding serves as the input to the first self-attention layer. The output from each self-attention layer is passed as input to the next layer as:

$$E_i = \text{Self Attention}(E_{i-1}), i \in \{1, 2, \dots, F\} \quad (2)$$

#### 3.2. Graph Feature Tuning (GFT)

Illustrated in Figure 4, GFT has three major components for fine-tuning. First, we prepend learnable continuous prompts to the sequential tokens so the graphs have a higher degree of freedom. Second, the graph features extractor, EdgeConv, extracts graph representations from the token embedding space. It takes input from the point tokenizer block and generates multi-layer graph features. We unlock the first layer of tokenizer to receive the parameter updates for unrestricted representation of the tokens. Third, we use cross-attention modules to inject features into the encoder. The features injection takes place sparsely to make it lightweight.

##### 3.2.1. Task-specific Learnable Prompt

Learnable prompt tuning is one of the efficient fine-tuning methods used in the 2D-vision and language domains to learn task-specific features [6, 14]. This extremely parameter-efficient method injects learnable continuous prompts into the token embedding space of the transformer while the entire encoder remains frozen. Similarly, we inject these learnable prompts to the initial embeddings  $E_0$  of Equation (1) between  $T_{cls}$  and other tokens as:

$$E_0 := \text{Inject}(E_0, P), \quad (3)$$

$$:= [T_{cls}; P; [T_1, T_2, \dots, T_L]], \quad (4)$$

$$:= [T_{cls}; [T_{P_1}, T_{P_2}, \dots, T_{P_s}]; [T_1, T_2, \dots, T_L]], \quad (5)$$

where,  $P \in \mathbb{R}^{s \times D}$  denotes learnable prompt and updated tokens representation  $E_0 \in \mathbb{R}^{(1+s+L) \times D}$ .

##### 3.2.2. EdgeConv Feature Extraction

EdgeConv [30] extracts features from the initial embedding matrix  $E_0$  (excluding the  $T_{cls}$  token) of the transformer pipeline. It is a component of multi-layered graph convolution functions for message passing that encodes features from the immediate neighbours. However,  $E_0$  does not contain the intrinsic neighbourhood information of a token. Thus, we define the locality information of  $i^{th}$  token  $T_i \in \mathbb{R}^{1 \times D}$  by grouping its  $K$ -nearest neighbours  $\mathcal{N}(T_i) \in \mathbb{R}^{K \times D}$ . Distance from the neighbours to  $T_i$  is attributed as edge features for KNN graphs, as shown in Figure 4 (b):

$$\mathcal{E}_i = \mathcal{N}(T_i) - T_i, \quad (6)$$

where  $\mathcal{E}_i \in \mathbb{R}^{K \times D}$ . We concatenate the  $\mathcal{E}_i$  with the central token  $T_i$  in the feature dimension, which gives us the neighbourhood information of  $T_i$  as  $\bar{\mathcal{N}}(T_i) \in \mathbb{R}^{K \times 2D}$ . Projecting the neighbourhood information to a latent space of  $d_1$  and pooling across  $K$  dimension, we get a new neighbourhood embedding of  $T_i$  as  $\mathbb{R}^{1 \times d_1}$ . We apply this for all  $(s+L)$  tokens to get the learned graph feature as  $M_1 \in \mathbb{R}^{(s+L) \times d_1}$ . This process is continued for multiple layers of latent spaces, creating a pyramid of graph features

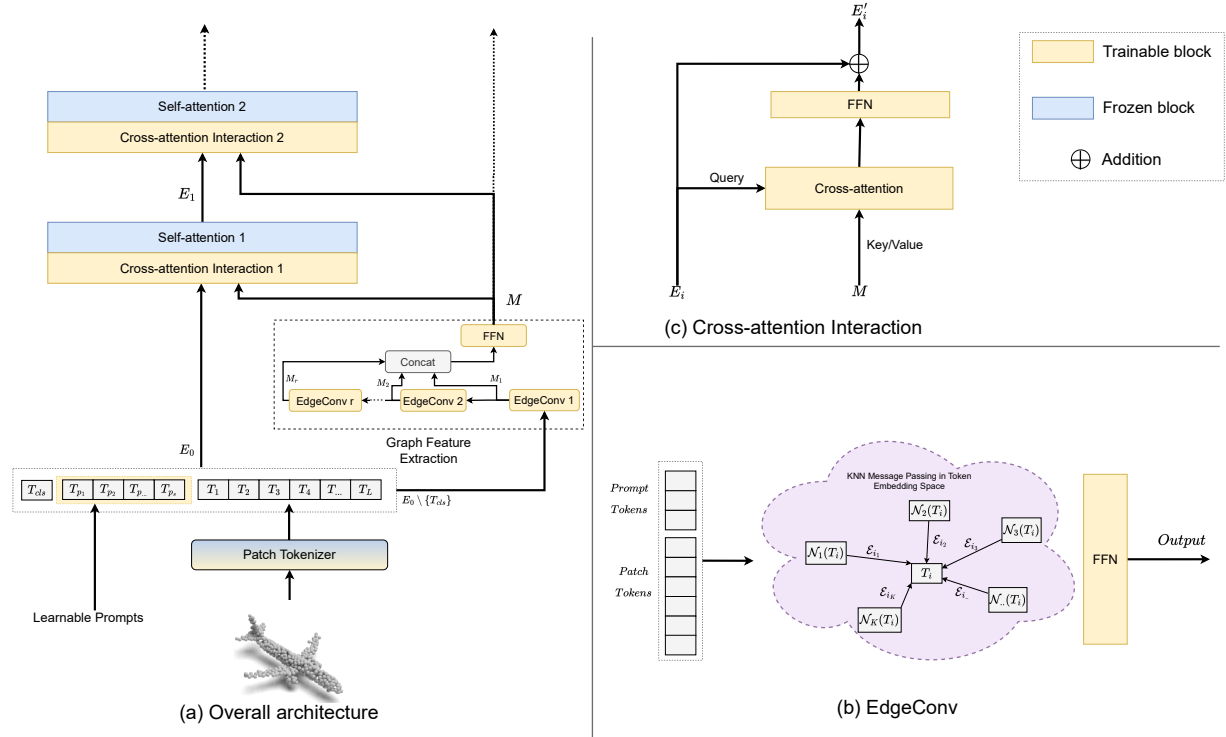


Figure 4. **Overall architecture of GFT.** (a) GFT is the composition of learnable prompts, graph feature extraction, and cross-attention interaction. (b) EdgeConv generates graph features from K-nearest neighbouring tokens, where the edge feature is  $\mathcal{E}_i = \mathcal{N}(T_i) - T_i$ . (c) Cross-attention interaction blocks use the encoder features  $E_i$  as query and the graph features  $M$  as key/value for the attention module.

$[M_1, M_2, \dots, M_r]$ , where  $r$  is the depth of the feature pyramid. These pyramid features are concatenated and fed to a feed-forward network (FFN) as:

$$M = FFN(Concat[M_1, M_2, \dots, M_r]) \quad (7)$$

where  $M \in \mathbb{R}^{(s+L) \times d}$  gives the final output of the EdgeConv network. For our experimentation, we work with  $r = 4$  and each feature dimension of 64 for the pyramid.

### 3.2.3. Cross-attention Interactions

Features from EdgeConv interact with the pretrained Point-Transformer to update the transformer’s features. Each interaction includes a cross-attention module [28] to fine-tune the pretrained features. To make the interaction lightweight, we implement sparse interaction to self-attention layers of point transformer. For instance, our implementation of  $F = 12$  layered encoders is subjected to 4 interactions at  $i \in \{1^{st}, 4^{th}, 7^{th}, 10^{th}\}$  self-attention layers.

At the input of  $i^{th}$  transformer encoder, the transformer embeddings  $E_{i-1}$  from the previous layer are updated by cross-attention modules operating with EdgeConv pyramid features  $M$ , where  $E_{i-1}$  and  $M$  are queries and keys features:

$$E'_{i-1} = XAttn(norm(E_{i-1}), norm(M)), \quad (8)$$

where  $norm(\cdot)$  is layer normalization and  $XAttn(a, b)$  is a cross-attention block,  $a$  denotes query, and  $b$  denotes key/value. The tensor shape of the embedding remains unchanged for use in the next encoder block.

## 4. Experimental Setup

### 4.1. Baseline PEFTs

To cover a wider spectrum of pretraining strategies for Point Transformer, we include three backbones: Point-BERT [37], Point-MAE [19], and ACT [5]. These foundation models were pretrained with ShapeNetCore from ShapeNet [2], containing  $\sim 51K$  CAD models of 55 common object categories. We include the results from two point-cloud-specific PEFTs, IDPT [38] and DAPT [44], to compare with our method.

### 4.2. Classification

For fair and robust comparison, we reproduce the results from IDPT [38] and DAPT [44] under the same experimental setting as ours. In Table 1, we report the average overall accuracy (OA%) of models with five consecutive seeds within  $[0, 4]$ . We design the task head to take inputs from CLS token  $T_{cls}$  and pooled prompt and patch tokens from the last layer of the transformer. Two datasets are used for

Method	Venue	#T-Params (M) $\downarrow$	FLOPs(G)	ScanObjectNN			ModelNet40
				OB_JBG	OBJ_ONLY	PB_T50_RS	
<i>Training with random weights initialization</i>							
PointNet [20]	CVPR'17	3.5	0.5	73.3	79.2	68.0	89.2
PointNet++ [21]	NeurIPS'17	1.5	1.7	82.3	84.3	77.9	90.7
DGCNN [30]	TOG'19	1.8	2.4	82.8	86.2	78.1	92.9
MVTN [8]	ICCV'21	11.2	43.7	-	-	82.8	93.8
PointNeXt [23]	NeurIPS'22	1.4	1.6	-	-	87.7	94.0
PointMLP [18]	ICLR'22	13.2	31.4	-	-	85.4	94.5
RepSurf-U [24]	CVPR'22	1.5	0.8	-	-	84.3	94.4
ADS [10]	ICCV'23	-	-	-	-	87.5	95.1
<i>Full fine-tuning (FFT) of pretrained models</i>							
OcCo [29]	ICCV'21	22.1	4.8	84.85	85.54	78.79	92.1
MaskPoint [17]	ECCV'22	22.1	-	89.70	89.30	84.60	93.8
Point-M2AE [39]	NeurIPS'22	15.3	3.6	91.22	88.81	86.43	94.0
ReCon[22]	ICML'23	43.6	5.3	94.15	93.12	89.73	93.9
Point-MAE [19]	ECCV'22	22.1	4.8	90.02	88.29	85.18	93.8
Point-BERT [37]	CVPR'22	22.1	4.8	87.43	88.12	83.07	93.2
ACT [5]	ICLR'23	22.1	4.8	93.29	91.91	88.21	93.7
<i>Parameter efficient fine-tuning (PEFT) with different backbones</i>							
Point-MAE backbone							
IDPT [38]	ICCV'23	1.70 (7.69%)	7.2	92.43 $\pm$ 0.27	91.43 $\pm$ 0.28	88.27 $\pm$ 0.23	93.00 $\pm$ 0.18
DAPT [44]	CVPR'24	1.10 (4.97%)	5.0	91.81 $\pm$ 0.36	91.36 $\pm$ 0.76	87.56 $\pm$ 0.64	92.88 $\pm$ 0.21
<b>GFT (Ours)</b>	-	<b>0.73 (3.26%)</b>	6.4	<b>92.56</b> $\pm$ 0.58	<b>91.46</b> $\pm$ 0.66	86.78 $\pm$ 0.32	<b>93.19</b> $\pm$ 0.19
Point-BERT backbone							
IDPT [38]	ICCV'23	1.70 (7.69%)	7.2	91.98 $\pm$ 0.76	91.67 $\pm$ 0.78	86.91 $\pm$ 0.78	92.67 $\pm$ 0.17
DAPT [44]	CVPR'24	1.10 (4.97%)	5.0	<b>93.05</b> $\pm$ 0.59	<b>91.67</b> $\pm$ 0.50	<b>88.63</b> $\pm$ 0.19	92.49 $\pm$ 0.08
<b>GFT (Ours)</b>	-	<b>0.73 (3.26%)</b>	6.4	92.36 $\pm$ 0.36	91.22 $\pm$ 0.32	87.37 $\pm$ 0.34	<b>93.01</b> $\pm$ 0.18
ACT backbone							
IDPT [38]	ICCV'23	1.70 (7.69%)	7.2	91.60 $\pm$ 0.39	<b>91.60</b> $\pm$ 0.37	<b>87.15</b> $\pm$ 0.39	<b>93.07</b> $\pm$ 0.20
DAPT [44]	CVPR'24	1.10 (4.97%)	5.0	91.15 $\pm$ 0.20	91.15 $\pm$ 0.52	86.97 $\pm$ 0.45	92.63 $\pm$ 0.21
<b>GFT (Ours)</b>	-	<b>0.73 (3.26%)</b>	6.4	<b>92.39</b> $\pm$ 0.48	91.26 $\pm$ 0.28	86.46 $\pm$ 0.43	93.07 $\pm$ 0.21

Table 1. **Overall accuracy (OA %  $\uparrow$ ) of classification on three variants of the ScanObjectNN [27] and the ModelNet40 [34].** #T-params and FLOPS (G) indicate the number of trainable parameters (in millions) and inference floating point operations, respectively. ScanObjectNN used the strong data augmentation mentioned by ACT [5].

evaluations: ScanObjectNN for real-world object classification and ModelNet-40 for synthetic object classification.

**ScanObjectNN** [27] is a real-world point cloud dataset containing scanned objects from indoor scenes. It consists of approximately 15K object scans with background clutter and occlusions, categorized into 15 object types. We use three dataset splits: OBJ\_BG, OBJ\_ONLY, and PB\_T50\_RS. For preprocessing, we sample 2K points per instance and apply a simple rotation, inspired by ACT [5].

**ModelNet-40** [34] consists of 12,311 CAD models of synthetic objects across 40 different categories. The point clouds in these models are clean, noise-free, and uniformly distributed with independent and identical distributions. Following the standard approach, we split the dataset into

9,843 instances for training and 2,468 for testing. During training, we sample 1K points from the distribution and apply random scaling and translation.

### 4.3. Segmentation

For segmentation, we design a transformer decoder with skip connections from the 3rd, 6th, 9th, and 11th layers of the pretrained model. Architecture used for the decoder of the segmentation is provide in the supplementary (Section 10). In line with the baseline papers IDPT [38] and DAPT [44], we report the best performance across ten consecutive seeds, [0, 9], as reproducing the baselines to compute mean metrics was computationally demanding. The evaluation dataset for the segmentation task is ShapeNet-Part.

**ShapeNetPart** [36] is a part segmentation dataset containing 50 different parts across 15 object categories. Following the standard benchmarking protocol [38, 44], we divide the dataset into training and test splits, consisting of 14K and 2.9K scans, respectively. Each data instance is represented by 2K sampled points.

#### 4.4. Implementation Details

We employed identical experimental settings to the PEFT methods for each baseline to ensure a fair comparison. All experiments are conducted on a single GeForce RTX 4090. Other hyperparameters regarding the fine-tuning tasks are mentioned in the supplementary (Section 9).

### 5. Results

**Real-World Object Classification.** The baseline foundational models favor clean and uniform point cloud data, similar to the pretraining dataset ShapeNet [2]. However, real-world point clouds have a different distribution due to noise, missing data, and non-uniform point density. Thus, we benchmark with ScanObjectNN [27].

As shown in Table 1, our method achieves an average performance gain of 4.12% over the FFT baseline of Point-BERT and 2.47% over Point-MAE. However, compared to the ACT baseline, there is an average performance drop of 0.5%. This could be attributed to ACT’s multi-stage pre-training [5], which, while effective, is computationally inefficient.

Notably, our method achieves competitive results with only 0.73% of the original parameter size. Compared to other PEFT methods, it outperforms most DAPT counterparts. While it does not surpass IDPT, it remains competitive. However, IDPT trains 1.7M parameters, more than twice the size of our model.

**Synthetic Objects Classification** ModelNet40 [34] contains synthetic models of objects. As illustrated in Table 1, our method does not exceed the FFT baselines of the pretrained backbones but remains competitive, with only a 0.5% average accuracy deficit. This finding of FFT can be attributed to the high similarity between the pretraining and fine-tuning datasets, as both consist of synthetic CAD models with a clean and uniform point distribution. Notably, our method outperforms other PEFT approaches across all three pretrained backbones.

**Few-shot Classification** Following previous works [5, 19, 37, 38, 44], we evaluate the pretrained model on  $N$ -way- $K$ -shot few-shot classification. In this setting,  $N \in \{5, 10\}$  represents the number of object categories, while  $K \in \{10, 20\}$  denotes the number of training instances

Method	5-way		10-way	
	10-shot	20-shot	10-shot	20-shot
<i>Full fine-tuning (FFT) of pretrained models</i>				
DGCNN-OcCo [29]	90.6 $\pm$ 2.8	92.5 $\pm$ 1.9	82.9 $\pm$ 1.3	86.5 $\pm$ 2.2
Transformer-OcCo [37]	94.0 $\pm$ 3.6	95.9 $\pm$ 2.3	89.4 $\pm$ 5.1	92.4 $\pm$ 4.6
MaskPoint [17]	95.0 $\pm$ 3.7	97.2 $\pm$ 1.7	91.4 $\pm$ 4.0	93.4 $\pm$ 3.5
EPCL [13]	95.1 $\pm$ 2.7	97.3 $\pm$ 1.6	91.1 $\pm$ 4.2	93.5 $\pm$ 3.8
Point-M2AE [39]	96.8 $\pm$ 1.8	98.3 $\pm$ 1.4	92.3 $\pm$ 4.5	95.0 $\pm$ 3.0
Point-MAE [19]	96.3 $\pm$ 2.5	97.8 $\pm$ 1.8	92.6 $\pm$ 4.1	95.0 $\pm$ 3.0
Point-BERT [37]	94.6 $\pm$ 3.1	96.3 $\pm$ 2.7	91.0 $\pm$ 5.4	92.7 $\pm$ 5.1
ACT [5]	96.8 $\pm$ 2.3	98.0 $\pm$ 1.4	93.3 $\pm$ 4.0	95.6 $\pm$ 2.8
<i>Parameter efficient fine-tuning (PEFT) with different backbones</i>				
Point-MAE backbone				
IDPT [38]	97.3 $\pm$ 2.1	97.9 $\pm$ 1.1	92.8 $\pm$ 4.1	95.4 $\pm$ 2.9
DAPT [44]	96.8 $\pm$ 1.8	98.0 $\pm$ 1.0	93.0 $\pm$ 3.5	95.5 $\pm$ 3.2
<b>GFT (Ours)</b>	96.3 $\pm$ 3.1	<b>98.3</b> $\pm$ 1.5	92.1 $\pm$ 5.3	95.1 $\pm$ 2.9
Point-BERT backbone				
IDPT [38]	96.0 $\pm$ 1.7	97.2 $\pm$ 2.6	91.9 $\pm$ 4.4	93.6 $\pm$ 3.5
DAPT [44]	95.8 $\pm$ 2.1	97.3 $\pm$ 1.3	92.2 $\pm$ 4.3	94.2 $\pm$ 3.4
<b>GFT (Ours)</b>	96.0 $\pm$ 2.5	<b>98.1</b> $\pm$ 1.3	92.2 $\pm$ 4.5	<b>94.5</b> $\pm$ 3.7
ACT backbone				
IDPT [38]	96.4 $\pm$ 2.5	98.3 $\pm$ 1.6	92.5 $\pm$ 4.5	95.6 $\pm$ 2.9
DAPT [44]	96.0 $\pm$ 3.0	97.4 $\pm$ 2.2	90.5 $\pm$ 4.9	94.2 $\pm$ 3.6
<b>GFT (Ours)</b>	96.0 $\pm$ 2.3	<b>98.3</b> $\pm$ 1.5	92.1 $\pm$ 5.0	95.0 $\pm$ 3.4

Table 2. **Few-shot learning on ModelNet40** [34]. We report the average overall accuracy (%) with the standard deviation (%) of 10 independent experiments.

per category. For example, a *5-way-10-shot* setup consists of five classes, each with ten training samples, totaling 50 training instances. We use a modified version of the ModelNet-40 [34] dataset for this task, where classes and training instances are sampled from its 40 categories.

As reported in Table 2, our method outperforms most existing FFT and PEFT approaches. While it may not surpass all PEFT baselines (IDPT and DAPT), across every  $N$ -way- $K$ -shot scenario, it achieves significant reductions of 57% and 34% in parameter space, respectively. Even in cases where performance lags slightly behind, the loss is negligible compared to the substantial improvement in parameter efficiency.

**Part Segmentation** We report the ShapeNetPart [36] segmentation performance of all of the fine-tuning approaches with mIoU of all classes and instances as in Table 3. Our method has 3.45 million parameters which is a  $\sim$ 40% reduction in the parameter size of the baseline methods, establishing itself as the most efficient method. Despite the smaller model size, GFT competes with the existing methods.

### 6. Ablation Studies

For the ablation study, we choose Point-MAE as the backbone, OBJ\_BG as the candidate classification task, and overall accuracy (OA%) as the evaluation metrics. Each

Method	#T-Params (M)	Cl. mIoU (%)	Inst. mIoU (%)
<i>Training with random weight initialization</i>			
PointNet [20]	-	80.39	83.7
PointNet++ [21]	-	81.85	85.1
DGCNN [30]	-	82.33	85.2
APES [31]	-	83.67	85.8
<i>Full fine-tuning (FFT) of pretrained models</i>			
OcCo [29]	27.09	83.42	85.1
MaskPoint [17]	-	85.60	86.0
ACT [5]	27.06	84.66	86.1
Point-BERT [37]	27.09	84.11	85.6
Point-MAE [19]	27.06	84.19	86.1
<i>Parameter efficient fine-tuning (PEFT) with different backbones</i>			
Point-BERT backbone			
IDPT [38]	5.69	83.50	85.3
DAPT [44]	5.65	<b>83.83</b>	<b>85.5</b>
<b>GFT (Ours)</b>	<b>3.84</b>	83.41	85.4
Point-MAE backbone			
IDPT [38]	5.69	83.79	<b>85.7</b>
DAPT [44]	5.65	84.01	<b>85.7</b>
<b>GFT (Ours)</b>	<b>3.84</b>	<b>84.05</b>	85.6

Table 3. **Part segmentation on the ShapeNetPart** [36]. The mIoU for all classes (Cl.) and instances (Inst.) are reported. #T-Params represents the trainable parameters.

EdgeConv	Cross-Attention	Learnable Prompts	#T-Params (M)	OA(%)
✗	✗	✗	0.30	87.26
✓	✗	✗	0.48	91.67
✓	✓	✗	0.62	91.81
✓	✗	✓	0.59	91.94
✓	✓	✓	0.73	<u>92.56</u>

Table 4. Analysis of the combination of GFT’s three different components from Section 3.2. Final combination of three gives the best performance.

experiment of Tables 4 and 5 and of Figure 5 is subjected to five consecutive seeds within  $[0, 4]$  for robust comparison. Underlined OA of the tables indicates the final settings of the reported results. Given the page limits, we have included the additional ablations of the individual components in the supplementary (Section 8).

**Analysis of Different Components.** We evaluate the impact of three key components in GFT: EdgeConv for graph feature extraction, cross-attention interaction, and task-specific learnable prompts. The performance of different component combinations is presented in Table 4.

Without these components, the model is equivalent to linear probing, where only the task head is fine-tuned, achieving an overall accuracy of 87.26%. Introducing the EdgeConv module significantly improves performance, yielding a 4.41% gain. EdgeConv has a receptive field of  $k = 20$ , which effectively incorporates the locality features. It proves to be highly effective on its own, and the addition

Layers	Interaction Type	#T-Params (M)	OA(%)
{1, 2, 3, 4}	Consecutive	0.73	91.98
{9, 10, 11, 12}	Consecutive	0.73	91.64
{1, 2, 3, .., 12}	Consecutive	1.08	92.56
{1, 4, 7, 10}	Sparse	0.73	<u>92.56</u>

Table 5. Analysis of cross-attention interaction at different layers of Point Transformer: Light sparse interactions achieve similar performance to heavy consecutive interactions.

of cross-attention interaction and learnable prompts further enhances accuracy. Specifically, integrating cross-attention with EdgeConv yields a further 0.14% improvement, underscoring the benefit of allowing encoder streams to selectively attend to graph features. Learnable prompts further enhance performance by 0.27%, as they offer a greater degree of freedom for graph construction. The final combination of all components achieves a total performance gain of 0.89% over EdgeConv-only variant, with only a minimal increase of 0.25 million trainable parameters.

**Analysis of Interaction Blocks.** We evaluate the sensitivity of the 12 encoder layers to graph features extracted from the EdgeConv module. To fine-tune the model, we design two types of cross-attention interactions: consecutive and sparse, as shown in Table 5. In consecutive interaction, graph features are injected into multiple consecutive layers, whereas in sparse interaction, they are introduced at non-adjacent layers. Table 5 shows that fine-tuning the first four layers {1, 2, 3, 4} improves performance by 0.34% compared to fine-tuning the last four layers {9, 10, 11, 12}. Since deeper layers in an encoder gradually learns features from coarse to fine, updating the coarse features seems efficacious to adapt new data distributions more effectively. While fine-tuning all layers may yield the best performance, it is often parameter-inefficient. Instead, sparsely updating a few layers, such as {1, 4, 7, 10}, achieves similar results.

**Parameters vs. Performance.** An important question to consider is: *What happens to performance when we reduce the parameters of existing PEFT methods to match those of GFT?* As shown in Figure 5, scaling down the parameters of DAPT and IDPT leads to a significant drop in overall accuracy (OA), whereas GFT remains more stable.

Specifically, when reducing the parameter count, IDPT experiences fluctuations of up to 0.97% in OA, while DAPT fluctuates by 0.51%. In contrast, GFT exhibits only a 0.37% variation, indicating greater stability to parameter reductions. Although DAPT’s fluctuation appears closer to GFT, its overall average performance remains lower, reinforcing the efficiency and stability of our method in achieving competitive results with fewer trainable parameters.

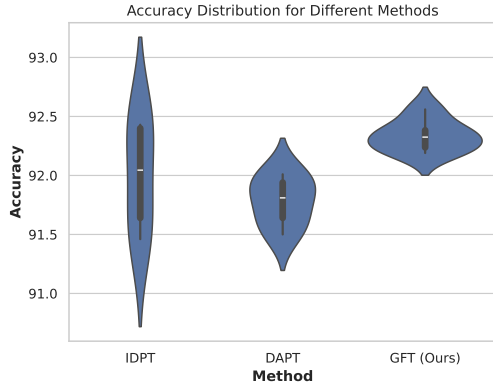


Figure 5. Violin plot comparing GFT and other PEFT methods across parameter sizes (0.6M, 1.7M) range. IDPT and DAPT display higher performance instability as parameters change, whereas GFT demonstrates greater immunity to parameter variation.

EdgeConv Dims.	Depth	#TP (M)	OA(%)
[32, 32, 32, 32]	4	0.66	92.25
[64, 64, 64]	3	0.71	91.77
[64, 64, 64, 64]	4	0.73	<u>92.56</u>
[64, 64, 64, 64]	5	0.76	91.77
[64, 128, 128, 64]	4	0.81	91.81
[128, 128, 128, 128]	4	0.92	92.19
[256, 256, 256, 256]	4	1.45	92.19

Table 6. Analysis of different dimensions of the EdgeConv feature pyramid. EdgeConv feature pyramid wider than 64 and deeper than 4 leads to overfitting of the fine-tuned tasks.

Cross-attention Dim.	#TP (M)	OA(%)
16	0.65	91.22
32	0.73	<u>92.56</u>
64	0.90	92.36
128	1.22	92.39

Table 7. Analysis of different dimensions of cross-attention interaction module. Increasing the dimension does not necessarily improve the performance.

**Analysis of EdgeConv Features.** We investigate the impact of varying the feature dimensions and the depth of the EdgeConv block pyramid, as shown in Table 6. Our results indicate that a depth of 4, with each layer having a feature dimension of 64, provides the optimal performance. Increasing the depth or widening the layers does not lead to further improvements, as the model begins to overfit.

**Analysis of Cross-attention Dimensions.** We analyze the impact of varying the dimensions of cross-attention

blocks on overall task performance in Table 7. Increasing the dimension from 16 to 32 results in a 1.34% improvement in accuracy. However, further increasing the dimension beyond 32 does not yield additional performance gains despite the rise in parameter count. Considering the balance between parameter efficiency and performance, we select 32 as the optimal dimension for our final experimental setup.

## 7. Conclusion and Limitation

In this paper, we introduce Graph Feature Tuning (GFT), a parameter-efficient fine-tuning method that encodes features in the token embedding space and injects them into transformer encoders. While our method does not outperform all existing approaches across every task, it remains competitive with state-of-the-art (SOTA) methods while significantly reducing the number of trainable parameters. Notably, when the parameters of SOTA methods are reduced to match GFT, they suffer a substantial drop in performance. This highlights the effectiveness of our approach, which leverages a combination of smaller components rather than relying on a single, large PEFT module.

Our findings also indicate the need for a better pre-training dataset than ShapeNet [7], which consists of synthetic data. While our method, along with other FFTs and PEFTs, performs well on downstream tasks involving synthetic datasets like ModelNet40 [34], its performance is less pronounced with real-world object scans from datasets such as ScanObjectNN [27]. This suggests that improving the pretraining process with a more diverse and representative distribution of real-world scans could further enhance the robustness and generalizability of these methods.

Leveraging graph features shows potential for improving segmentation tasks; however, our current work includes only a basic evaluation, leaving room for more in-depth and comprehensive analysis in future research. Also, our method introduces additional inference FLOPs after fine-tuning. In the future, we can work with adaptation method similar to LoRA that add zero inference latency.

## Acknowledgement

Research was sponsored by the Army Research Laboratory and was accomplished under Cooperative Agreement Number W911NF-23-2-0224. The views and conclusions contained in this document are those of the authors and should not be interpreted as representing the official policies, either expressed or implied, of the Army Research Laboratory or the U.S. Government. The U.S. Government is authorized to reproduce and distribute reprints for Government purposes notwithstanding any copyright notation herein.

## References

[1] Rabin Adhikari, Safal Thapaliya, Manish Dhakal, and Bishesh Khanal. Tunevlseg: Prompt tuning benchmark for vision-language segmentation models. In *Proceedings of the Asian Conference on Computer Vision*, pages 126–144, 2024. 2

[2] Angel X. Chang, Thomas A. Funkhouser, Leonidas J. Guibas, Pat Hanrahan, Qi-Xing Huang, Zimo Li, Silvio Savarese, Manolis Savva, Shuran Song, Hao Su, Jianxiong Xiao, Li Yi, and Fisher Yu. Shapenet: An information-rich 3d model repository. *CoRR*, abs/1512.03012, 2015. 4, 6

[3] Alexis Conneau, Holger Schwenk, Loïc Barrault, and Yann Lecun. Very deep convolutional networks for text classification. *arXiv preprint arXiv:1606.01781*, 2016. 2

[4] Manish Dhakal, Rabin Adhikari, Safal Thapaliya, and Bishesh Khanal. Vlsm-adapter: Finetuning vision-language segmentation efficiently with lightweight blocks. In *International Conference on Medical Image Computing and Computer-Assisted Intervention*, pages 712–722. Springer, 2024. 2

[5] Runpei Dong, Zekun Qi, Linfeng Zhang, Junbo Zhang, Jian-jian Sun, Zheng Ge, Li Yi, and Kaisheng Ma. Autoencoders as cross-modal teachers: Can pretrained 2d image transformers help 3d representation learning? In *The Eleventh International Conference on Learning Representations*, 2023. 1, 2, 4, 5, 6, 7, 11

[6] Tianyu Gao, Adam Fisch, and Danqi Chen. Making pre-trained language models better few-shot learners. In *Proceedings of the 59th Annual Meeting of the Association for Computational Linguistics and the 11th International Joint Conference on Natural Language Processing (Volume 1: Long Papers)*. Association for Computational Linguistics, 2021. 2, 3

[7] Ross Girshick, Jeff Donahue, Trevor Darrell, and Jitendra Malik. Rich feature hierarchies for accurate object detection and semantic segmentation. In *Proceedings of the IEEE conference on computer vision and pattern recognition*, pages 580–587, 2014. 8

[8] Abdullah Hamdi, Silvio Giancola, and Bernard Ghanem. Mvtn: Multi-view transformation network for 3d shape recognition. In *Proceedings of the IEEE/CVF International Conference on Computer Vision*, pages 1–11, 2021. 5

[9] Kaiming He, Xiangyu Zhang, Shaoqing Ren, and Jian Sun. Deep residual learning for image recognition. In *Proceedings of the IEEE conference on computer vision and pattern recognition*, pages 770–778, 2016. 2

[10] Cheng-Yao Hong, Yu-Ying Chou, and Tyng-Luh Liu. Attention discriminant sampling for point clouds. In *Proceedings of the IEEE/CVF International Conference on Computer Vision*, pages 14429–14440, 2023. 5

[11] Neil Houlsby, Andrei Giurgiu, Stanislaw Jastrzebski, Bruna Morrone, Quentin De Laroussilhe, Andrea Gesmundo, Mona Attariyan, and Sylvain Gelly. Parameter-efficient transfer learning for nlp. In *International conference on machine learning*, pages 2790–2799. PMLR, 2019. 1, 2

[12] Edward J Hu, Yelong Shen, Phillip Wallis, Zeyuan Allen-Zhu, Yuanzhi Li, Shean Wang, Lu Wang, Weizhu Chen, et al. Lora: Low-rank adaptation of large language models. *ICLR*, 1(2):3, 2022. 2

[13] Xiaoshui Huang, Sheng Li, Wentao Qu, Tong He, Yifan Zuo, and Wanli Ouyang. Frozen clip model is an efficient point cloud backbone. *arXiv preprint arXiv:2212.04098*, 2022. 6

[14] Menglin Jia, Luming Tang, Bor-Chun Chen, Claire Cardie, Serge Belongie, Bharath Hariharan, and Ser-Nam Lim. Visual prompt tuning. In *European Conference on Computer Vision*, pages 709–727. Springer, 2022. 1, 2, 3

[15] Nal Kalchbrenner, Edward Grefenstette, and Phil Blunsom. A convolutional neural network for modelling sentences. In *Proceedings of the 52nd Annual Meeting of the Association for Computational Linguistics (Volume 1: Long Papers)*, pages 655–665, 2014. 2

[16] Dingkang Liang, Xin Zhou, Wei Xu, Xingkui Zhu, Zhikang Zou, Xiaoqing Ye, Xiao Tan, and Xiang Bai. Pointmamba: A simple state space model for point cloud analysis. *Advances in neural information processing systems*, 37:32653–32677, 2025. 1

[17] Haotian Liu, Mu Cai, and Yong Jae Lee. Masked discrimination for self-supervised learning on point clouds. In *European Conference on Computer Vision*, pages 657–675. Springer, 2022. 1, 5, 6, 7

[18] Xu Ma, Can Qin, Haoxuan You, Haoxi Ran, and Yun Fu. Rethinking network design and local geometry in point cloud: A simple residual MLP framework. In *International Conference on Learning Representations*, 2022. 5

[19] Yatian Pang, Wenxiao Wang, Francis EH Tay, Wei Liu, Yonghong Tian, and Li Yuan. Masked autoencoders for point cloud self-supervised learning. In *European conference on computer vision*, pages 604–621. Springer, 2022. 1, 2, 4, 5, 6, 7, 11

[20] Charles R Qi, Hao Su, Kaichun Mo, and Leonidas J Guibas. Pointnet: Deep learning on point sets for 3d classification and segmentation. In *Proceedings of the IEEE conference on computer vision and pattern recognition*, pages 652–660, 2017. 1, 5, 7

[21] Charles Ruizhongtai Qi, Li Yi, Hao Su, and Leonidas J Guibas. Pointnet++: Deep hierarchical feature learning on point sets in a metric space. *Advances in neural information processing systems*, 30, 2017. 1, 2, 5, 7

[22] Zekun Qi, Runpei Dong, Guofan Fan, Zheng Ge, Xiangyu Zhang, Kaisheng Ma, and Li Yi. Contrast with reconstruct: Contrastive 3d representation learning guided by generative pretraining. In *International Conference on Machine Learning*, pages 28223–28243. PMLR, 2023. 2, 5

[23] Guocheng Qian, Yuchen Li, Houwen Peng, Jinjie Mai, Hasan Hammoud, Mohamed Elhoseiny, and Bernard Ghanem. Pointnext: Revisiting pointnet++ with improved training and scaling strategies. *Advances in neural information processing systems*, 35:23192–23204, 2022. 5

[24] Haoxi Ran, Jun Liu, and Chengjie Wang. Surface representation for point clouds. In *Proceedings of the IEEE/CVF conference on computer vision and pattern recognition*, pages 18942–18952, 2022. 5

[25] Sylvestre-Alvise Rebuffi, Hakan Bilen, and Andrea Vedaldi. Learning multiple visual domains with residual adapters. Ad-

*vances in neural information processing systems*, 30, 2017. 2

[26] Taylor Shin, Yasaman Razeghi, Robert L Logan IV, Eric Wallace, and Sameer Singh. Autoprompt: Eliciting knowledge from language models with automatically generated prompts. In *Proceedings of the 2020 Conference on Empirical Methods in Natural Language Processing (EMNLP)*, pages 4222–4235, 2020. 2

[27] Mikaela Angelina Uy, Quang-Hieu Pham, Binh-Son Hua, Thanh Nguyen, and Sai-Kit Yeung. Revisiting point cloud classification: A new benchmark dataset and classification model on real-world data. In *Proceedings of the IEEE/CVF international conference on computer vision*, pages 1588–1597, 2019. 5, 6, 8

[28] Ashish Vaswani, Noam Shazeer, Niki Parmar, Jakob Uszkoreit, Llion Jones, Aidan N Gomez, Łukasz Kaiser, and Illia Polosukhin. Attention is all you need. *Advances in neural information processing systems*, 30, 2017. 1, 2, 4

[29] Hanchen Wang, Qi Liu, Xiangyu Yue, Joan Lasenby, and Matt J Kusner. Unsupervised point cloud pre-training via occlusion completion. In *Proceedings of the IEEE/CVF international conference on computer vision*, pages 9782–9792, 2021. 2, 5, 6, 7

[30] Yue Wang, Yongbin Sun, Ziwei Liu, Sanjay E Sarma, Michael M Bronstein, and Justin M Solomon. Dynamic graph cnn for learning on point clouds. *ACM Transactions on Graphics (tog)*, 38(5):1–12, 2019. 1, 2, 3, 5, 7

[31] Chengzhi Wu, Junwei Zheng, Julius Pfrommer, and Jürgen Beyerer. Attention-based point cloud edge sampling. In *Proceedings of the IEEE/CVF Conference on Computer Vision and Pattern Recognition*, pages 5333–5343, 2023. 7

[32] Wenxuan Wu, Zhongang Qi, and Li Fuxin. Pointconv: Deep convolutional networks on 3d point clouds. In *Proceedings of the IEEE/CVF Conference on computer vision and pattern recognition*, pages 9621–9630, 2019. 2

[33] Yichen Wu, Hongming Piao, Long-Kai Huang, Renzhen Wang, Wanhua Li, Hanspeter Pfister, Deyu Meng, Kede Ma, and Ying Wei. S-lora: Scalable low-rank adaptation for class incremental learning, 2025. 2

[34] Zhirong Wu, Shuran Song, Aditya Khosla, Fisher Yu, Lin-guang Zhang, Xiaoou Tang, and Jianxiong Xiao. 3d shapenets: A deep representation for volumetric shapes. In *Proceedings of the IEEE conference on computer vision and pattern recognition*, pages 1912–1920, 2015. 5, 6, 8

[35] Saining Xie, Jiatao Gu, Demi Guo, Charles R Qi, Leonidas Guibas, and Or Litany. Pointcontrast: Unsupervised pre-training for 3d point cloud understanding. In *Computer Vision–ECCV 2020: 16th European Conference, Glasgow, UK, August 23–28, 2020, Proceedings, Part III 16*, pages 574–591. Springer, 2020. 1

[36] Li Yi, Vladimir G Kim, Duygu Ceylan, I-Chao Shen, Mengyan Yan, Hao Su, Cewu Lu, Qixing Huang, Alla Sheffer, and Leonidas Guibas. A scalable active framework for region annotation in 3d shape collections. *ACM Transactions on Graphics (ToG)*, 35(6):1–12, 2016. 6, 7

[37] Xumin Yu, Lulu Tang, Yongming Rao, Tiejun Huang, Jie Zhou, and Jiwen Lu. Point-bert: Pre-training 3d point cloud transformers with masked point modeling. In *Proceedings of the IEEE/CVF conference on computer vision and pattern recognition*, pages 19313–19322, 2022. 1, 2, 4, 5, 6, 7, 11

[38] Yaohua Zha, Jinpeng Wang, Tao Dai, Bin Chen, Zhi Wang, and Shu-Tao Xia. Instance-aware dynamic prompt tuning for pre-trained point cloud models. In *ICCV*, 2023. 1, 2, 3, 4, 5, 6, 7, 11

[39] Renrui Zhang, Ziyu Guo, Peng Gao, Rongyao Fang, Bin Zhao, Dong Wang, Yu Qiao, and Hongsheng Li. Point-m2ae: multi-scale masked autoencoders for hierarchical point cloud pre-training. *Advances in neural information processing systems*, 35:27061–27074, 2022. 2, 5, 6

[40] Yabin Zhang, Jiehong Lin, Ruihuang Li, Kui Jia, and Lei Zhang. Point-dae: Denoising autoencoders for self-supervised point cloud learning. *CoRR*, 2022. 2

[41] Zaiwei Zhang, Rohit Girdhar, Armand Joulin, and Ishan Misra. Self-supervised pretraining of 3d features on any point-cloud. In *Proceedings of the IEEE/CVF International Conference on Computer Vision*, pages 10252–10263, 2021. 2

[42] Hengshuang Zhao, Li Jiang, Jiaya Jia, Philip HS Torr, and Vladlen Koltun. Point transformer. In *Proceedings of the IEEE/CVF international conference on computer vision*, pages 16259–16268, 2021. 2, 3

[43] Kaiyang Zhou, Jingkang Yang, Chen Change Loy, and Ziwei Liu. Learning to prompt for vision-language models. *International Journal of Computer Vision*, 130(9):2337–2348, 2022. 2

[44] Xin Zhou, Dingkang Liang, Wei Xu, Xingkui Zhu, Yihan Xu, Zhikang Zou, and Xiang Bai. Dynamic adapter meets prompt tuning: Parameter-efficient transfer learning for point cloud analysis. In *CVPR*, 2024. 1, 2, 4, 5, 6, 7, 11

# GFT: Graph Feature Tuning for Efficient Point Cloud Analysis

## Supplementary Material

Learnable Prompt Length	#TP (M)	OA(%)
10	0.72	91.91
25	0.72	91.74
50	0.73	<u>92.56</u>
100	0.75	92.05

Table 8. Analysis of prompt length for GFT analysis. Prompt length beyond 50 hurts the performance.

EdgeConv KNN	Training Complexity		OA(%)
	Epoch Time (secs)	Memory (GB)	
5	15.5	6.9	91.77
10	16.5	7.1	91.67
20	18.0	8.7	<u>92.56</u>
40	23.5	10.4	92.22

Table 9. Analysis of different dimensions of the EdgeConv feature pyramid. Increasing the neighbours in KNN imposes higher training time and memory complexities.

## 8. Additional Ablation Study

Similar to the ablation study in the main paper, we use Point-MAE as the pretrained backbone and OBJ\_BG as the downstream classification task; each experimentation is subjected to five different seed values.

**Prompt Length vs. Performance.** As shown in Table 8, we evaluate the sensitivity of our method to prompt length by experimenting with four different values:  $\{10, 25, 50, 100\}$ . The optimal performance is achieved with a prompt length of 50, which we use for our reported results. Increasing the prompt length does not necessarily yield better performance. Unlike patch tokens, these prompts lack locality information but offer greater degrees of freedom in graph construction. However, an excessive number of prompts may introduce unnecessary edges, which could negatively impact downstream tasks.

**EdgeConv KNN** The performance of GFT is also influenced by the number of neighbors used for message passing. Changing the number of neighbors does not affect the trainable parameters but changes the time and computational complexities. To analyze this, we conduct an ablation study with different values of  $k \in \{5, 10, 20, 40\}$  in KNN, as shown in Table 9. Given 50 prompt tokens and 128 patch tokens, we have a total of 178 tokens and mes-

Feature Pooling Techniques		#TP (M)	OA(%)
$T_{cls}$	Patch Pooling	0.54	90.29
✓	✓	0.64	91.98
✓	✓	✓	0.73 <u>92.56</u>

Table 10. Analysis of token projections for classification task. The combinationion of all of the feature pooling gives the best result.

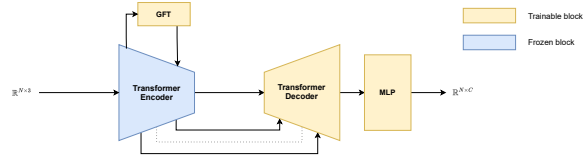


Figure 6. **Overall architecture of the segmentation model.** The segmentation head utilizes intermediate features from the encoder layers, processes them through transformer decoders, and finally passes them to an MLP layer to predict the class labels.

sage passing with the 20 nearest neighbors yields the best results. While increasing the number of neighbors raises both time and memory complexity, it does not lead to further improvements in performance.

**Tokens Projections for Task Head** We explore combinations of three options for projecting features from Point Transformers for classification:  $T_{cls}$ , patch pooling, and prompt pooling. Previous fine-tuning methods primarily relied on  $T_{cls}$  and patch pooling as projections for the task head [5, 19, 37, 38, 44]. However, GFT has learnable prompts where task-specific features are accumulated. We achieve the best results by leveraging all three projection options, as shown in Table 10.

## 9. Training Details

Table 11 provides the comprehensive training details for our method across different classification and segmentation tasks. Classification models have been optimized using cross-entropy loss, while segmentation models utilize negative log-likelihood loss. We follow a similar training approach to earlier PEFT methods [38, 44].

## 10. Architecture for Segmentation Head

Our part segmentation task head consists of two main components: (1) a transformer decoder, composed of stacked

Configuration	Classification			Segmentation (ShapeNetPart)
	ScanObjectNN	ModelNet	ModelNet Few-shot	-
Optimizer	AdamW	AdamW	AdamW	AdamW
Learning rate (LR)	5e-4	5e-4	1e-3	2e-4
LR scheduler	Cosine	Cosine	Cosine	Cosine
Warmup LR	1e-6	1e-6	1e-6	1e-6
Warmup epochs	10	10	10	10
Minimum LR	1e-6	1e-6	1e-6	1e-6
Weight decay	5e-2	5e-2	1e-4	5e-2
Training epochs	300	300	150	300
Batch size	32	32	32	32
Number of points	2048	1024	1024	2048
Number of patches/tokens	128	64	64	128
Point patch size	32	32	32	32
<i>GFT Configurations</i>				
Learnable prompt length	50	50	50	50
EdgeConv KNN size	20	20	20	20
EdgeConv feat dims.	[64, 64, 64, 64]	[64, 64, 64, 64]	[64, 64, 64, 64]	[64, 64, 64, 64]
EdgeConv FFN dim	256	256	256	256
Cross-attention dim	32	32	32	32
Cross-attention heads	2	2	1	2

Table 11. Training details for the fine-tuning tasks.

self-attention blocks, which receives input from the encoder representations through skip connections and down-projection layers; and (2) a multi-layer perceptron (MLP) that outputs class predictions for each point, producing a tensor of shape  $\mathbb{R}^{N \times C}$ , where  $N$  is the number of points and  $C$  is the number of classes as given in Figure 6.

## 11. Vizualization of Attention Maps

As shown in the Figure 7, during fine-tuning of the pre-trained backbones, we analyze the attention maps from patch tokens to the CLS token ( $T_{cls}$ ). When the pretrained weights are kept frozen, fine-tuning the task-level graph features guides the attention to consistently focus on discriminative regions. For example, attention maps for cones highlight the apex, while those for chairs emphasize the backrest. In contrast, the pretrained model often struggles to identify a consistent region of interest—sometimes focusing on one part of the object, and other times on another—indicating a lack of clear task-specific understanding.

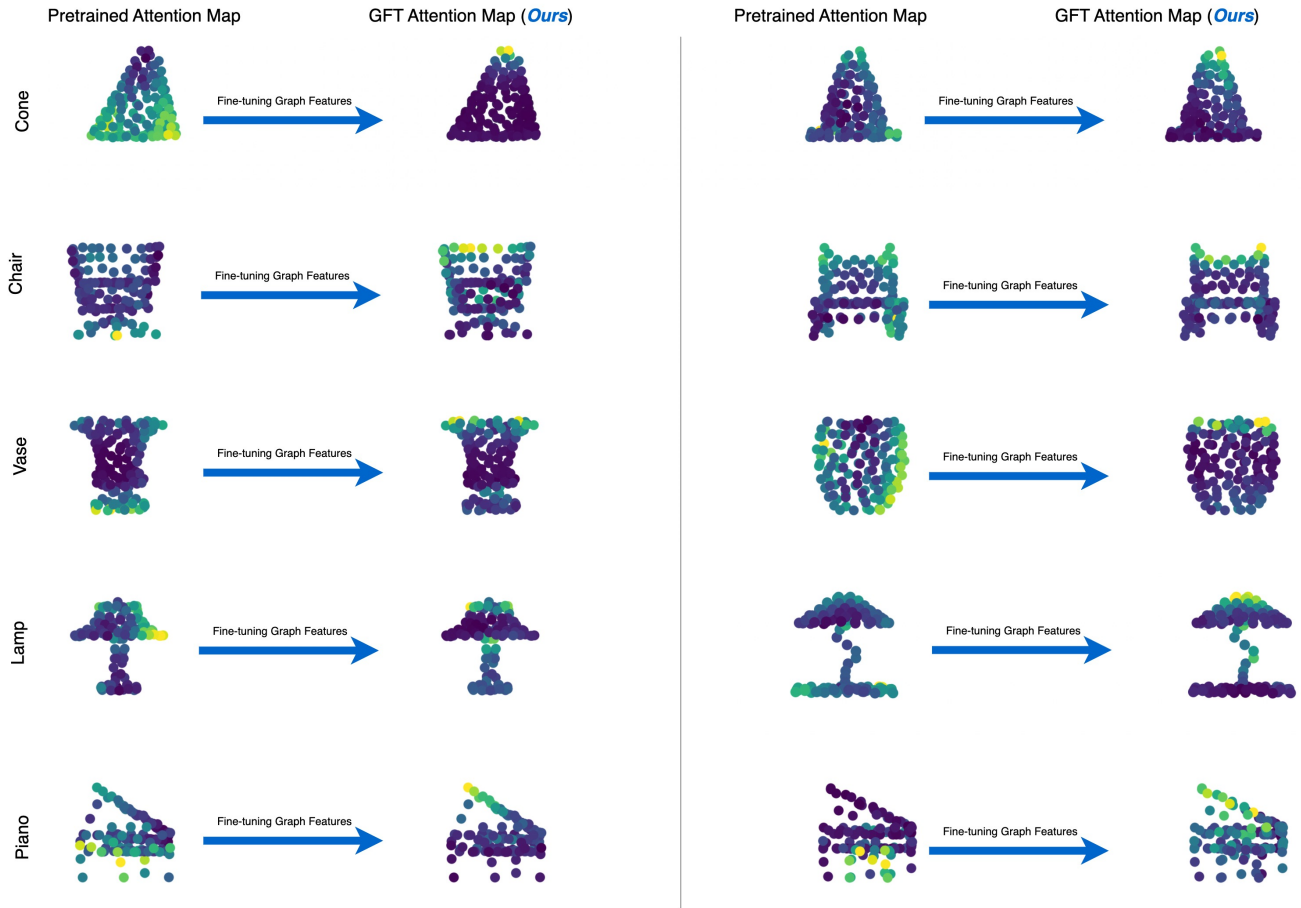


Figure 7. Fine-tuning leads to a shift in attention, redirecting focus from arbitrary regions to task-relevant, discriminative parts of the objects—such as the backrest for chairs, apex for cones, mouth for vases, and fallboard for pianos. In contrast, the pretrained model exhibits uncertainty, with attention scattered across different parts.